Exploring transverse pattern formation in a dual-polarization self-mode-locked monolithic Yb: KGW laser and generating a 25-GHz sub-picosecond vortex beam via gain competition

M. T. Chang,[1] H. C. Liang,[2] K. W. Su,[1] and Y. F. Chen[1,*]

[1]*Department of Electrophysics, National Chiao Tung University, Hsinchu 30010, Taiwan*
[2]*Institute of Optoelectronic Science, National Taiwan Ocean University, Keelung 20224, Taiwan*
[*]*yfchen@cc.nctu.edu.tw*

Abstract: Formation of transverse modes in a dual-polarization self-mode-locked monolithic Yb: KGW laser under high-power pumping is thoroughly explored. It is experimentally observed that the polarization-resolved transverse patterns are considerably affected by the pump location in the transverse plane of the gain medium. In contrast, the longitudinal self-mode-locking is nearly undisturbed by the pump position, even under the high-power pumping. Under central pumping, a vortex beam of the Laguerre-Gaussian $LG_{p,l}$ mode with p = 1 and l = 1 can be efficiently generated through the process of the gain competition with a sub-picosecond pulse train at 25.3 GHz and the output power can be up to 1.45 W at a pump power of 10.0 W. Under off-center pumping, the symmetry breaking causes the transverse patterns to be dominated by the high-order Hermite-Gaussian modes. Numerical analyses are further performed to manifest the symmetry breaking induced by the off-center pumping.

OCIS codes: (140.3580) Lasers, solid-state; (140.3480) Lasers, diode-pumped; (140.4050) Mode-locked lasers; (140.3615) Lasers, ytterbium.

References and links

1. J. Z. Sotor, G. Dudzik, and K. M. Abramski, "Single frequency, monolithic Nd:YVO_4/YVO_4/KTP diode pumped solid state laser optimization by parasitic oscillations elimination," Opt. Commun. **291**, 279–284 (2013).
2. D. W. Chen, C. L. Fincher, T. S. Rose, F. L. Vernon, and R. A. Fields, "Diode-pumped 1-W continuous-wave Er:YAG 3-mum laser," Opt. Lett. **24**(6), 385–387 (1999).
3. Y. J. Chen, Y. F. Lin, J. H. Huang, X. H. Gong, Z. D. Luo, and Y. D. Huang, "Diode-pumped monolithic Er^{3+}:Yb^{3+}:$YAl_3(BO_3)_4$ micro-laser at 1.6 μm," Opt. Commun. **285**(5), 751–754 (2012).
4. T. R. Schibli, T. Kremp, U. Morgner, F. X. Kärtner, R. Butendeich, J. Schwarz, H. Schweizer, F. Scholz, J. Hetzler, and M. Wegener, "Continuous-wave operation and Q-switched mode locking of Cr^{4+}:YAG microchip lasers," Opt. Lett. **26**(12), 941–943 (2001).
5. C. Y. Cho, P. H. Tuan, Y. T. Yu, K. F. Huang, and Y. F. Chen, "A cryogenically cooled Nd:YAG monolithic laser for efficient dual-wavelength operation at 1061 and 1064 nm," Laser Phys. Lett. **10**(4), 045806 (2013).
6. are S. Zhou, S. Li, K. K. Lee, and Y. C. Chen, "Monolithic self-Q-switched Cr,Nd:YAG laser," Opt. Lett. **18**(7), 511–512 (1993).
7. Y. C. Chen, S. Li, K. K. Lee, and S. Zhou, "Self-stabilized single-longitudinal-mode operation in a self-Q-switched Cr,Nd:YAG laser," Opt. Lett. **18**(17), 1418–1419 (1993).
8. R. S. Conroy, T. Lake, G. J. Friel, A. J. Kemp, and B. D. Sinclair, "Self-Q-switched Nd:YVO_4 microchip lasers," Opt. Lett. **23**(6), 457–459 (1998).
9. J. Dong, K. Ueda, A. Shirakawa, H. Yagi, T. Yanagitani, and A. A. Kaminskii, "Composite Yb:YAG/Cr^{4+}:YAG ceramics picosecond microchip lasers," Opt. Express **15**(22), 14516–14523 (2007).
10. N. Pavel, M. Tsunekane, and T. Taira, "Composite, all-ceramics, high-peak power Nd:YAG/$Cr^{(4+)}$:YAG monolithic micro-laser with multiple-beam output for engine ignition," Opt. Express **19**(10), 9378–9384 (2011).
11. W. Z. Zhuang, M. T. Chang, H. C. Liang, and Y. F. Chen, "High-power high-repetition-rate subpicosecond monolithic Yb:KGW laser with self-mode locking," Opt. Lett. **38**(14), 2596–2599 (2013).
12. C. Y. Lee, C. C. Chang, H. C. Liang, and Y. F. Chen, "Frequency comb expansion in a monolithic self-mode-locked laser concurrent with stimulated Raman scattering," Laser Photonics Rev. **8**(5), 750–755 (2014).

#260585 Received 4 Mar 2016; revised 7 Apr 2016; accepted 10 Apr 2016; published 13 Apr 2016

13. Y. F. Chen, M. T. Chang, W. Z. Zhuang, K. W. Su, K. F. Huang, and H. C. Liang, "Generation of sub-terahertz repetition rates from a monolithic self-mode-locked laser coupled with an external Fabry-Perot cavity," Laser Photonics Rev. **9**(1), 91–97 (2015).
14. M. T. Chang, H. C. Liang, K. W. Su, and Y. F. Chen, "Dual-comb self-mode-locked monolithic Yb:KGW laser with orthogonal polarizations," Opt. Express **23**(8), 10111–10116 (2015).
15. J. J. Zayhowski and A. Mooradian, "Single-frequency microchip Nd lasers," Opt. Lett. **14**(1), 24–26 (1989).
16. J. J. Zayhowski and A. Mooradian, "Frequency-modulated Nd:YAG microchip lasers," Opt. Lett. **14**(12), 618–620 (1989).
17. G. J. Dixon, L. S. Lingvay, and R. H. Jarman, "Properties of close-coupled, monolithic lithium neodymium tetraphosphate laser," Proc. SPIE **1104**, 107–112 (1989).
18. P. A. Loiko, V. E. Kisel, N. V. Kondratuk, K. V. Yumashev, N. V. Kuleshov, and A. A. Pavlyuk, "14 W high-efficiency diode-pumped cw Yb:KGd(WO_4)$_2$ laser with low thermo-optic aberrations," Opt. Mater. **35**(3), 582–585 (2013).
19. M. Woerdemann, C. Alpmann, M. Esseling, and C. Denz, "Advanced optical trapping by complex beam shaping," Laser Photonics Rev. **7**(6), 839–854 (2013).
20. M. C. Cross and P. C. Hohenberg, "Pattern formation outside of equilibrium," Rev. Mod. Phys. **65**(3), 851–1112 (1993).
21. A. Y. Okulov, "3D-vortex labyrinths in the near field of solid-state microchip laser," J. Mod. Opt. **55**(2), 241–259 (2008).
22. V. Y. Bazhenov, M. S. Soskin, and M. V. Vasnetsov, "Screw Dislocations in Light Wavefronts," J. Mod. Opt. **39**(5), 985–990 (1992).
23. E. Abramochkin and V. Volostnikov, "Beam transformations and nontransformed beams," Opt. Commun. **83**(1-2), 123–135 (1991).
24. D. Naidoo, K. Aït-Ameur, M. Brunel, and A. Forbes, "Intra-cavity generation of superpositions of Laguerre–Gaussian beams," Appl. Phys. B **106**(3), 683–690 (2012).
25. T. Kuga, Y. Torii, N. Shiokawa, T. Hirano, Y. Shimizu, and H. Sasada, "Novel optical trap of atoms with a doughnut beam," Phys. Rev. Lett. **78**(25), 4713–4716 (1997).
26. Z. Chen, M. Segev, D. W. Wilson, R. E. Muller, and P. D. Maker, "Self-trapping of an optical vortex by use of the bulk photovoltaic effect," Phys. Rev. Lett. **78**(15), 2948–2951 (1997).
27. C. L. Tang and H. Statz, "Maximum-emission principle and phase-locking in multimode lasers," J. Appl. Phys. **38**(7), 2963–2968 (1967).
28. H. Statz, "On the conditions for self-locking of modes in lasers," J. Appl. Phys. **38**(12), 4648–4655 (1967).
29. P. A. Loiko, K. V. Yumashev, N. V. Kuleshov, and A. A. Pavlyuk, "Comparative thermal analysis of Nd- and Yb-doped YAG and KGdW laser crystals under diode- and flashlamp-pumping," Opt. Laser Technol. **44**(7), 2232–2237 (2012).
30. A. K. Cousins, "Temperature and thermal stress scaling in finite-lengthend-pumped laser rods," IEEE J. Quantum Electron. **28**(4), 1057–1069 (1992).
31. M. E. Innocenzi, H. T. Yura, C. L. Fincher, and R. A. Fields, "Thermal modeling of continuous-wave end-pumped solid-state lasers," Appl. Phys. Lett. **56**(19), 1831–1833 (1990).

1. Introduction

Monolithic or bonded resonators offer the advantage of mechanical stability, compact, and alignment-free manufacturing as compared to conventional laser cavities which typically require many precisely aligned parts. Monolithic cavity configurations have been used to achieve the continuous-wave [1–5], Q-switched [6–10], and self-mode-locked operations [11–14]. Zayhowski and Mooradian [15, 16] and Dixon *et al.* [17] almost simultaneously found that the thermally induced lens in the gain medium plays a decisive role in bringing the flat–flat cavity into geometrical stability. This finding indicates that the formation of transverse modes in high-power monolithic crystal lasers is mainly determined by the thermal lensing effect.

Recently, a dual-polarization self-mode-locked Yb:KGd(WO_4)$_2$ (Yb:KGW) laser has been realized in a monolithic configuration [14] with the cutting angle along the N_g direction and the polarized states along the N_p and N_m directions. It has also been confirmed that the N_g -cut Yb:KGW crystal can offer positive thermal lensing with weak astigmatism [18]. In addition to the thermal lensing effect, the gain competition between two orthogonal polarization states is expected to lead to a rich variety of transverse pattern formation under the high-power pumping. Although formation of transverse modes in laser systems has been extensively studied due to practical applications and academic interests [19–21], the mode variations in a dual-polarization self-mode-locked monolithic laser under high-power pumping have not been explored.

In this work, the polarization-resolved transverse modes are experimentally explored in a high-power dual-polarization self-mode-locked Yb:KGW laser under the impacts of gain

#260585 Received 4 Mar 2016; revised 7 Apr 2016; accepted 10 Apr 2016; published 13 Apr 2016

competition and thermal lensing effect. Based on thoroughly experimental observations, the polarization-resolved output powers and transverse patterns are confirmed to be significantly dependent on the pump location in the transverse plane of the gain medium. When the pump beam is in the central region with a radius of approximately 0.4 mm, both transverse modes of two orthogonally polarized states are found to exhibit nearly circular characteristics. In contrast, when the pump beam is outside the central region of the gain medium, the transverse patterns display the feature of high-order HG modes for high-power pumping. In the time domain, it is confirmed that longitudinal self-mode-locking always remains unchanged for all the pump powers. The most interesting observation is that under central pumping a vortex beam of the Laguerre-Gaussian $LG_{p,l}$ mode with $p = 1$ and $l = 1$ can be generated with pulse duration of 0.98 ps and pulse repetition rate of 25.3 GHz, where p and l are the radial and azimuthal indices. The maximum output power for the $LG_{1,1}$ mode can be up to 1.45 W under a pump power of 10.0 W. Since the $LG_{1,1}$ mode possesses well-defined angular momentum, the present finding may be practically useful in the optomechanical applications [22–26]. Finally, we numerically analyze the influence of the pump location on the temperature distribution of the laser crystal to disclose the symmetry breaking induced by the off-center pumping.

2. Experimental setup

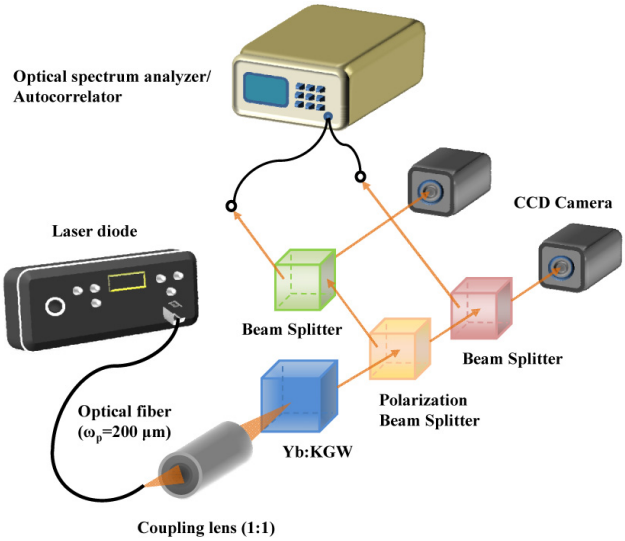

Fig. 1. Experimental setup for the polarization-resolved measurement of the high-power dual-polarization self-mode-locked Yb:KGW laser.

Figure 1 depicts the experimental setup for the polarization-resolved measurement of the high-power dual-polarization self-mode-locked Yb:KGW laser. The pump source was a 980-nm fiber-coupled laser diode with a core diameter of 200 μm and a numerical aperture of 0.2. A set of lenses with 1.0 magnification was used to re-image the pump beam into the laser crystal. The gain medium was an Yb-doped (5.0 at. %) N_g-cut KGW crystal with dimension approximately 3 × 3 × 3 mm^3. The crystal was wrapped with indium foil and was placed within a water-cooled copper heat sink. The water temperature was precisely maintained at 8.0 ± 0.2 °C to ensure stable output. The Yb:KGW crystal was coated to form a monolithic flat-flat cavity. The input surface of the laser crystal has a coating for high reflection (R > 99.8%) from 1040 nm to 1070 nm and high transmission (T > 95%) at 980 nm to serve as a front mirror. The other facet has a coating for partial reflection (R ≈98.5%) within 1040-1070 nm to serve as an output mirror and has a coating for high reflection (R > 99%) at 980 nm to obtain the double-passing absorption.

#260585 Received 4 Mar 2016; revised 7 Apr 2016; accepted 10 Apr 2016; published 13 Apr 2016

The polarization-resolved transverse patterns were measured with charge-coupled device cameras (MODEL C2741-03, HAMAMATSU PHOTONICS). The polarization-resolved first-order autocorrelation traces were measured with a Michelson optical interferometer (Advantest Q8347). The polarization-resolved wavelength spectra were acquired with a resolution of 0.003 nm by performing Fourier transform for the experimental first-order autocorrelation traces. The temporal behavior of the laser output was analyzed by exploiting a commercial autocorrelator (APE GmbH, PulseCheck) to obtain the second-order autocorrelation. In the following, experimental results obtained with the pump beam within and outside the central region are presented, respectively, to reveal the dependence of the transverse patterns on the pump location.

3. Output characteristics under central pumping

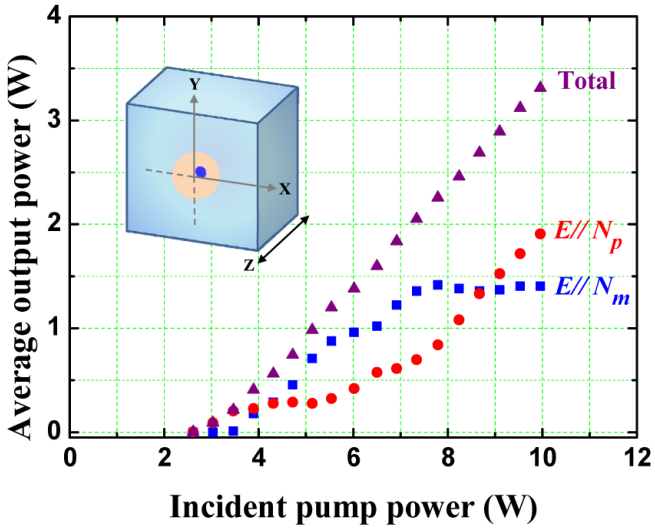

Fig. 2. Polarization-resolved and total output powers versus incident pump power for the pump beam in the central region.

The laser can be working and stable in the mode-locked regime for the whole range of given pump. The measurements limited to 10 W of pump power are mainly subject to the thermally induced fracture in the gain medium. It is observed that the laser crystal will exhibit the phenomenon of the fracture in the long time operation when the pump power exceeds 11 W. Figure 2 shows the polarization-resolved and the total output powers versus the incident pump power for the gain medium to be pumped in the central region. The total output power could be up to 3.4 W at a pump power of 10.0 W, corresponding to a slope efficiency of 45.3% and an optical-to-optical efficiency of 34.0%. The threshold pump powers were approximately 2.5 W and 3.0 W for the polarization states parallel to the N_p and N_m directions, respectively. It can be seen that the output powers of two orthogonal polarization components are nearly equal to 0.24 W and 1.4 W at the incident pump powers of 4.3 W and 8.7 W, respectively. Note that the output reflectivity must be as high as 98.5% for obtaining the dual-polarization operation [14]. It was found that the output was a single polarization state for the output reflectivity to be 95% at the lasing wavelength [11]. Figure 3 shows experimental results for the polarization-resolved transverse patterns and lasing wavelength spectra for different pump powers. Experimental results revealed that the transverse pattern in the N_p polarized state was mainly dominated by the $TEM_{0,0}$ fundamental mode for the incident pump power P_{in} from the threshold power 2.5 W to 10.0 W, as seen in Fig. 3. On the other hand, the transverse pattern in the N_m polarized state was observed to change from the $TEM_{0,0}$ mode for the pump power in the range 3.0–5.2 W to the $LG_{1,0}$ mode for the pump

#260585 Received 4 Mar 2016; revised 7 Apr 2016; accepted 10 Apr 2016; published 13 Apr 2016

power in the range 5.4–8.2 W. More intriguingly, the transverse pattern in the N_m polarized state was nearly governed by the $LG_{1,1}$ mode for the pump power in the range 8.4–10.0 W. Some typical transverse patterns are shown in Fig. 3.

The causes of the mode change in the N_m polarized state comprise the thermal lensing and the gain competition. The thermal lensing effect results in the shrinkage of the cavity mode size and leads to the excitation of the higher order modes because the pump size becomes larger than the cavity mode size. Since the gain of the N_p polarized state is slightly higher than that of the N_m polarized state, the central part of the pump distribution is mainly utilized by the N_p polarized state with the fundamental mode. Therefore, the feasible method to obtain the dual-polarization $TEM_{0,0}$ operation for high power regime is to reduce the thermal lensing effect by decreasing the dopant concentration and slightly increasing the crystal length. On the other hand, the possible way to obtain $LG_{0,1}$ doughnut mode is to finely tune the pump size.

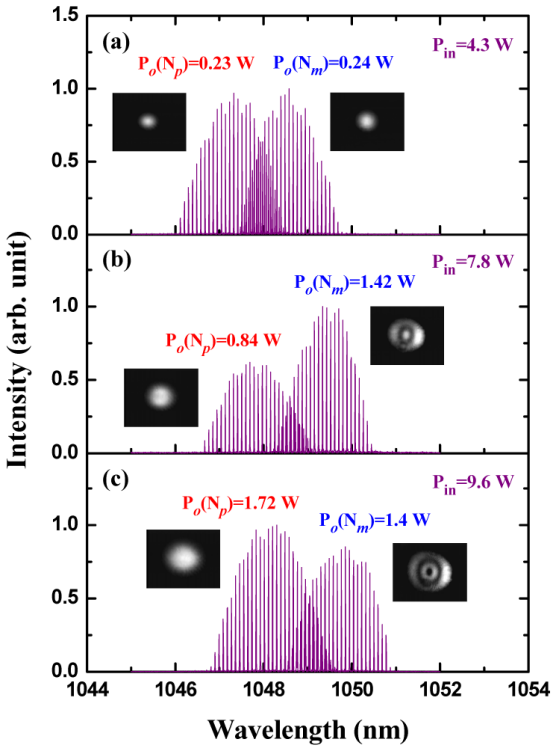

Fig. 3. Polarization-resolved transverse patterns and lasing spectral combs at three pump powers for manifesting the variation of transverse modes on the pump power.

The polarization-resolved optical spectra for several pump powers are also plotted in Fig. 3. The structures of frequency combs for two orthogonally polarized states can be clearly seen. For the pump power increasing from 4.3 W to 9.6 W, the central frequency of the N_p polarized state is gradually red-shifted from 1047.3 nm to 1048.2 nm and that of the N_m polarized state red-shifted from 1048.5 nm to 1049.5 nm. The bandwidths of the lasing spectra in the full width at half maximum (FWHM) are generally in the range of 1.6–1.8 nm for both orthogonal polarization states. Using the experimental spectra, the longitudinal mode intervals for the N_p and N_m polarized states are calculated to be 25.8 GHz and 25.3 GHz, respectively. The obtained mode intervals agree very well with the free spectral ranges of the Yb:KGW crystal for the N_p and N_m polarizations. More importantly, the comb structure nearly remained unchanged even when the lasing mode of the N_m polarized state became $LG_{1,0}$ or $LG_{1,1}$ mode. In other words, the high-power pumping only leads two orthogonally polarized

#260585 Received 4 Mar 2016; revised 7 Apr 2016; accepted 10 Apr 2016; published 13 Apr 2016

states to emit different transverse modes but does not considerably affect the longitudinal mode-locking.

The first- and second-order autocorrelations were measured to evaluate the characteristics of the time domain. It is found that experimental data for the first- and second-order autocorrelations of two orthogonally polarized states are nearly independent of the pump power in the whole investigated range. These observations once again verify the operation of longitudinal self-mode-locking. The mechanism of the stability in the present self-mode-locking is conjectured to come from the large mode spacing that avoids the interaction of the mode coupling. Furthermore, the phase locking between the multi-longitudinal modes is convinced by the maximum-emission principle [27]. From the viewpoint of the time domain, the shorter roundtrip time is beneficial to the achievement of the self-mode-locking [28]. Unlike the conventional Kerr-lens mode-locking, the stability is strongly dependent on the intensity of the self-focusing within gain medium. This is also the reason why the appearance of higher transverse modes does not affect the self-mode-locking operation. Experimental results for the polarization-resolved first-order autocorrelation trace at the maximum pump power of 10.0 W are shown in Figs. 4(a) and 4(b). The pulse repetition rates can be confirmed by using the crystal length of 2.93 mm and the group indexes of 1.986 for the N_p polarization and 2.023 for the N_m polarization. Figures 4(c) and 4(d) depict the FWHM widths of the polarization-resolved single pulses in the second-order autocorrelation traces at the maximum pump power of 10.0 W. The pulse widths are evaluated by assuming the Gaussian-shaped temporal profile and are found to be approximately 0.96 ps and 0.98 ps for the N_p and N_m polarizations, respectively. Using the measured spectral bandwidths, the time-bandwidth products can be calculated to be approximately 0.46 for both orthogonally polarized states. This result is a little larger than the Fourier- transform limit of 0.441. The frequency chirping mainly arises from the group velocity dispersion of the gain medium. To the best of our knowledge, this is the first time that a vortex beam of the $LG_{1,1}$ mode with a 25.3-GHz sub-picosecond pulse train is generated through the gain competition between two orthogonal polarization states in the self-mode-locked operation. Furthermore, the maximum output power for the $LG_{1,1}$ mode can be up to 1.45 W at a pump power of 10.0 W. The helical phase front of the LG_{11} mode can be measured by using a configuration of Mach–Zehnder interferometer. The result is shown in Fig. 5.

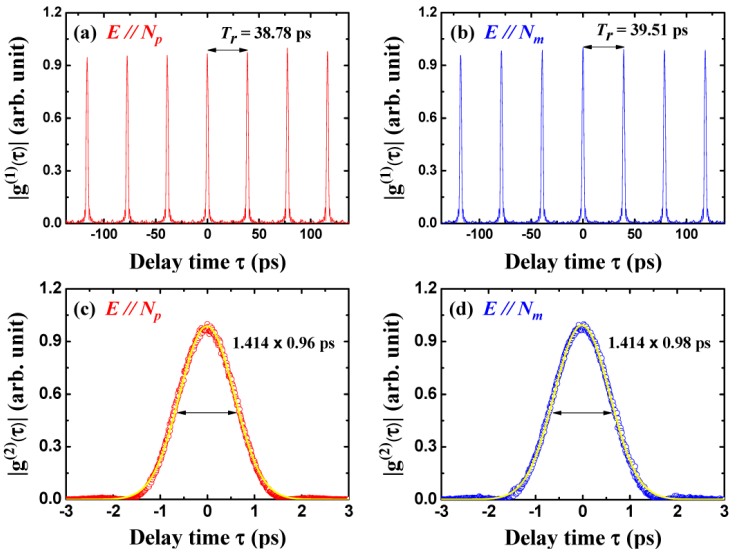

Fig. 4. Polarization-resolved first-order autocorrelation traces at the maximum pump power of 10.0 W for the N_p polarized state (a) and N_m polarized state (b); FWHM widths of the polarization-resolved single pulses in the second-order autocorrelation traces at the maximum pump power of 10.0 W for the N_p polarized state (c) and N_m polarized state (d).

#260585 Received 4 Mar 2016; revised 7 Apr 2016; accepted 10 Apr 2016; published 13 Apr 2016

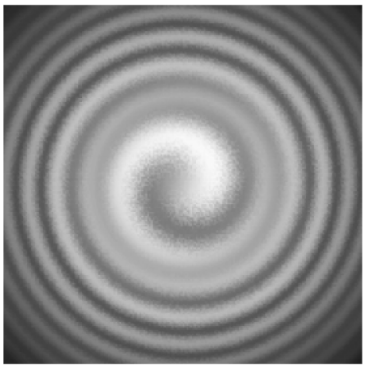

Fig. 5. Helical phase front of the LG_{11} mode.

4. Output characteristics under off-center pumping

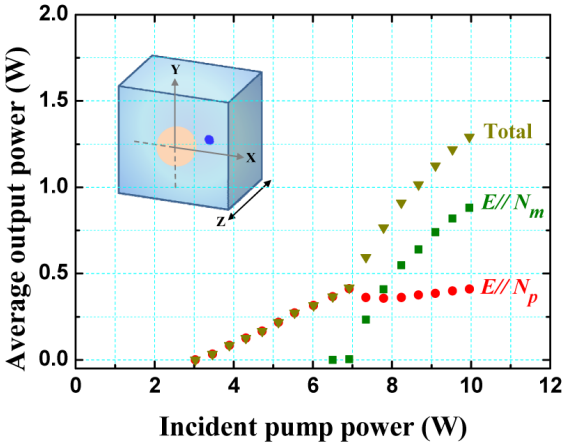

Fig. 6. Polarization-resolved and total output powers versus incident pump power for the pump beam outside the central region with d_x = 1.0 mm and d_y = 0.5 mm.

Without loss of generality, experimental results obtained with the pump position at d_x = 1.0 mm and d_y = 0.5 mm are given to manifest the influence of the pump position, where d_x and d_y are the distances away from the transverse center of the gain medium in the horizontal and vertical directions, respectively. Figure 6 shows the polarization-resolved and the total output powers versus the incident pump power. In comparison with the results shown in Fig. 2 for the central pumping, the overall efficiency has decreased by nearly 50%. Besides, although the pump threshold for the N_p polarized state is almost unchanged, the threshold power for the N_m polarized state has significantly increased up to 6.5 W. Namely, the output emission is linearly polarized in the N_p direction for the pump power less than 6.5 W. Under this circumstance, the transverse mode is mainly dominated by $TEM_{0,0}$ mode, as shown in Fig. 7(a). When the N_m polarized state starts to get lasing for the pump power higher than 6.5 W, the transverse patterns for the N_p and N_m polarized states are found to be $HG_{0,1}$ and $HG_{2,0}$ modes, respectively, as shown in Figs. 7(b) and 7(c). Even though the circular symmetry of the transverse structures is breaking due to the off-center pumping, the feature of frequency combs still maintains for two orthogonally polarized states, as seen in Fig. 7. The first- and second-order autocorrelations were also measured to confirm that the operation of longitudinal self-mode-locking could be achieved in the whole investigated range of the pump power. To sum up, the off-center pumping only affects the transverse patterns for two

#260585 Received 4 Mar 2016; revised 7 Apr 2016; accepted 10 Apr 2016; published 13 Apr 2016

orthogonally polarized states but does not destroy the operation of the longitudinal self-mode-locking.

We further compute the temperature distribution $T(x,y,z)$ arising from the absorbed pump power to explore the symmetry breaking induced by the off-center pumping. In the steady-state case, the heat conduction equation for $T(x,y,z)$ is given by

$$\nabla\cdot(\vec{K}_c\nabla T)=-Q(x,y,z), \tag{1}$$

where $\vec{K}_c$ is the thermal conductivity tensor and $Q(x,y,z)$ is the heat source density in the laser crystal. Using the Gaussian distribution to model the pump beam, the heat source density can be generalized as

$$Q(x,y,z)=\frac{2\xi P_{abs}}{\pi\omega_p^2}\frac{\alpha}{1-e^{-\alpha l}}e^{-\alpha z}\,e^{-2(x-d_x)^2/\omega_p^2}\,e^{-2(y-d_y)^2/\omega_p^2}. \tag{2}$$

where P_{abs} is the absorbed pump power, ξ is the thermal loading factor, α is the absorption coefficient, ω_p is the radius of the pump beam, and l is the crystal length. The thermal conductivity tensor $\vec{K}_c$ is diagonal in the frame of optical indicatrix axes N_p, N_m, and N_g. The thermal conductivity coefficients are 2.5, 3.0, and 3.5 W/m·K in the directions of N_p, N_m, and N_g, respectively [29]. For conventional edge cooling, the boundary conditions of the end surfaces can be approximated as adiabatic due to the fact that the cooling-surface convection coefficient is three orders of magnitude larger than the natural convection coefficient on the end surfaces [30, 31]. Under this approximation and using the expansion method, the temperature distribution were numerically calculated with the parameters of ξ = 0.05, ω_p = 200 μm, α = 1.2 mm^{-1}, and l = 3 mm.

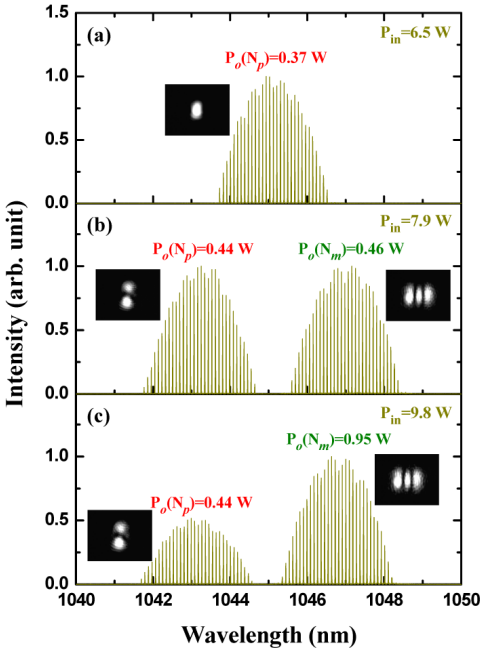

Fig. 7. Polarization-resolved transverse patterns and lasing spectral combs at three pump powers for manifesting the variation of transverse modes on the pump power for the case of off-center pumping.

#260585 Received 4 Mar 2016; revised 7 Apr 2016; accepted 10 Apr 2016; published 13 Apr 2016

Figure 8 shows the calculated results for temperature profiles at the input face of the laser crystal at an absorption power of 6 W for three different pump positions with d_x = 0.0, 0.5, and 1.0 mm and d_y = 0.0 mm for all cases. The symmetry breaking of the temperature profile caused by the off-center pumping can be clearly seen. Using the numerical calculation, it is found that for the case shown in Fig. 6, the center of the thermal lensing is outside the pump location with distances of approximately 100 μm and 170 μm along the x and y directions, respectively. This mismatch causes the appearance of the high order transverse modes not only in the N_m but also in the N_p polarized states.

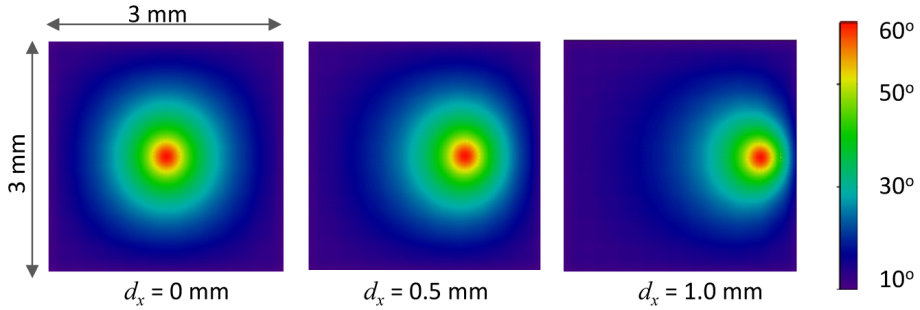

Fig. 8. calculated results for temperature profiles at the input face of the laser crystal at an absorption power of 6 W for three different pump positions with d_x = 0.0, 0.5, and 1.0 mm and d_y = 0.0 mm for all cases.

5. Conclusion

We have experimentally explored the impacts of the gain competition and the thermal lensing on the transverse pattern formation in a dual-polarization self-mode-locked monolithic Yb:KGW laser. It is observed that not only the polarization-resolved transverse patterns but also the output powers notably depend on the pump location in the transverse plane of the gain medium. The transverse patterns of two orthogonally polarized states generally display nearly circular features for the pump beam in the central region with a radius of approximately 0.4 mm, whereas these symmetries are broken to be the high-order HG modes for the pump beam outside the central region. We also find that the longitudinal self-mode-locking is almost not affected by the high-power pumping and the pump position. Consequently, a vortex beam of the $LG_{1,1}$ mode with a sub-picosecond pulse train at 25.3 GHz can be stably generated through the process of the gain competition between two orthogonal polarization states. Under a pump power of 10.0 W, the output power of the $LG_{1,1}$ mode can achieve 1.45 W. This finding is probably beneficial to the optomechanical applications because of the well-defined angular momentum of the $LG_{1,1}$ beam.

Acknowledgments

The authors thank the Ministry of Science and Technology of Taiwan for the financial support of this research under Contract No. MOST 103-2112-M-009-0016-MY3.

#260585 Received 4 Mar 2016; revised 7 Apr 2016; accepted 10 Apr 2016; published 13 Apr 2016